Available online at www.sciencedirect.com
SCIENCE DIRECT®
ELSEVIER
Nuclear Instruments and Methods in Physics Research B 219–220 (2004) 810–814
NIM B
Beam Interactions with Materials & Atoms
www.elsevier.com/locate/nimb

Atomic transport in insulators under high-flux heavy-ion implantation

N. Kishimoto [a,*], O.A. Plaksin [a,b], N. Umeda [c], Y. Takeda [a]

[a] *Nanomaterials Laboratory, National Institute for Materials Science, 3-13 Sakura, Tsukuba, Ibaraki 305-0003, Japan*
[b] *SSC RF-A. I. Leypunsky Institute of Physics and Power Engineering, Obninsk 249033, Russia*
[c] *Institute of Materials Science, University of Tsukuba, Tsukuba, Ibaraki 305-8573, Japan*

Abstract

Although ion implantation has a unique merit in fabricating immiscible metal–insulator composites being promising for non-linear optical applications, high-flux implantation especially is subject to pronounced atomic transports, either inside or outside the solid. Negative Cu ions of 60 keV irradiated substrates of a-SiO_2 and $MgO \cdot 2.4(Al_2O_3)$ at fluxes up to 100 μA/cm^2. Atomic redistribution of Cu nanoparticles inside the substrate was observed by cross-sectional TEM. Atomic release of Cu implants out of the substrate was detected by ion-induced photon spectroscopy, with fast-response CCD cameras. Spontaneous metal precipitation in insulators is attained at high flux. The ion-induced photon spectra of a-SiO_2 consist of sharp line spectra and a broad luminescence. The presence of line spectra demonstrated the outward transport into vacuum and loss of Cu atoms via the surface to the vacuum. Cations in $MgO \cdot 2.4(Al_2O_3)$ are also significantly released to the vacuum via the surface. The outward mass transport results from ion-induced sputtering/sublimation of implants, concurrently with radiation-induced diffusion towards the surface.

PACS: 25.75.q; 32.80.t; 61.46.w; 71.23.Cq; 78.40.q
Keywords: Heavy ion; Nanoparticle; Atomic transport; Silica glass; Ion-induced photon

1. Introduction

Heavy-ion implantation is a superb tool to fabricate nanoparticles of immiscible metal elements in insulators which show non-linear ultrafast optical response associated with surface plasmon resonance [1,2]. Usage of negative ions exercises their power in alleviating surface charging of insulators in balance with secondary electron emission [3] and enables us to widen the applicable flux range up to high fluxes, e.g. 10^2 μA/cm^2 [4]. High-flux implantation provides merits of efficient doping for precipitation, spontaneous metal precipitation without post-implantation annealing and occasionally a self-assembled two-dimensional structure of nanoparticles, such as in amorphous (a-)SiO_2 [5,6]. The in-beam processes dynamically take place not only in recoil events but also in ion-induced diffusion and precipitation, mostly due to the electronic-energy deposition as in insulators [7]. The enhanced diffusion causes

* Corresponding author. Tel.: +81-29-863-5433; fax: +81-29-863-5571.
E-mail address: kishimoto.naoki@nims.go.jp (N. Kishimoto).

0168-583X/$ - see front matter © 2004 Elsevier B.V. All rights reserved.
doi:10.1016/j.nimb.2004.01.168

Ostwald ripening of nanoparticles suitable for non-linear optical applications [8] but the high-flux implantation concurrently causes atomic rearrangement deviating from the predicted profile, such as bimodal implant distributions along depth [9,10].

Accordingly, high-flux implantation, particularly at low energy (<several tens keV), is subjected to pronounced atomic transports, either inside or outside the solid. Understanding the kinetic processes is requisite to control nanoparticle composites. The diffusion-related processes are, more or less, material-dependent, such as a radiation-induced viscous flow in a-SiO_2 [11] and strong recombination of radiation-induced defects in $MgAl_2O_4$ [12]. It is desired to understand both material-dependent- and universal phenomena.

In this paper, we discuss in-beam atomic transports in a-SiO_2 and non-stoichiometric spinel $MgO \cdot n(Al_2O_3)$ ($n = 2.4$) by comparing between the inside nanoparticle morphology by TEM and the outside atomic release by ion-induced photon spectroscopy, by the aid of the TRIM [13] and TRIDYN codes [14].

2. Experimental procedures

Specimens used are a-SiO_2 (KU-1®, OH^-: 820 ppm) and single-crystal spinel $MgO \cdot 2.4(Al_2O_3)$ of (1 0 0)-plane. The disk substrates, polished to the optical grade, are 15 mm in diameter and 0.5 mm in thickness. Negative Cu ions of 60 keV were implanted into substrates at various fluxes up to about 100 μA/cm^2, to a fluence of 3.0×10^{17} ions/cm^2. The negative ion techniques and the apparatus were described elsewhere [4]. The projected ranges of 60 keV Cu in SiO_2 and $MgO \cdot 2.4(Al_2O_3)$ are 45 and 30 nm, respectively [13]. Depth profiles of 60 keV Cu with increasing the fluence were estimated with the TRIDYN code [14]. To ensure thermal contact of a specimen to the water-cooled stage, we used a contact mask of a 12 mm-diameter-aperture. Specimen temperature was monitored by a thermocouple attached to periphery of the substrate and did not exceed 500 K below 100 μA/cm^2. Time-resolved optical devices, with fast-response CCD cameras (Princeton Instruments: IMAX-512), were used for ion-induced photon spectroscopy. The full detection range was from 900 to 200 nm. To eliminate ion-induced emission from the surrounding of a specimen, the beam cross-section was shaped into a 12 mm-diameter circle through a pre-aperture, which was aligned onto the same area of the substrate surface with the Cu contact aperture. After the in situ experiments, cross-sectional TEM was conducted to evaluate microstructures in the Cu-implanted region.

3. Results and discussion

Nanoparticle morphology is dominated by atomic transports as a function of ion energy, fluence, flux and substrate species, etc. Here, we focus on atomic transport after the recoil events, which is both material-dependent and flux-dependent. One of the most contrasting cases so far seen is the case of a-SiO_2 versus $MgO \cdot 2.4(Al_2O_3)$. Fig. 1(a) and (b) present cross-sectional TEM images of a-SiO_2 and $MgO \cdot 2.4(Al_2O_3)$ implanted with 60 keV Cu^- at 10 μA/cm^2 to 3.0×10^{16} ions/cm^2, where the area is near the projected range. The Cu^- implantation at 10 μA/cm^2 causes spontaneous precipitation of spherical nanoparticles with ~10 nm in diameter, which is suitable for non-linear optical applications in the visible light range. The roundness of nanoparticles promptly indicates a mechanism of surface-tension-limited growth (Ostwald ripening) under pronounced radiation-induced diffusion. On the other hand, the

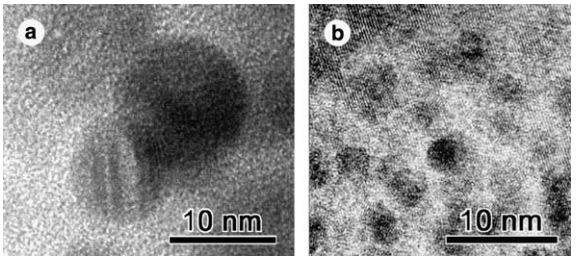

Fig. 1. Cross-sectional TEM images of a-SiO_2 (a) and $MgO \cdot 2.4(Al_2O_3)$ (b) implanted with 60 keV Cu^- at 10 μA/cm^2 to 3.0×10^{16} ions/cm^2, where the area is taken near the projected range.

implantation of the same condition causes much smaller precipitation in $MgO \cdot 2.4(Al_2O_3)$, as seen in Fig. 1(b). The smaller and denser precipitation in $MgO \cdot 2.4(Al_2O_3)$ is ascribed to less Cu diffusion without coarsening the size. The material-dependence of precipitation can be used to controlling particle size, as well as the flux dependence.

The strong Cu diffusion in a-SiO_2 is preferable for nanoparticle precipitation but also leads to depth rearrangement along with the depth. Figs. 2(a)–(c) show depth profiles of Cu atoms (in nanoparticles) in a-SiO_2 at 3 μA/cm^2 (a), 45 μA/cm^2 (b) and in $MgO \cdot 2.4(Al_2O_3)$ at 50 μA/cm^2 (c). At low fluxes <10 μA/cm^2 in a-SiO_2, the Cu atomic profile agrees with the TRIM prediction [13], that is, no anomalous atomic transports occur. With increasing flux, the profile of Cu atoms shifts towards the surface and becomes narrower in depth [5]. The shallowing effect on the Cu profile was observed above ~10 μA/cm^2, without losing implants. As seen in Fig. 2(b), the Cu profile becomes very narrow at 45 μA/cm^2, and results in two-dimensional distribution of Cu nanoparticles [5]. The general trend of the implant profile in the TRIDYN regime is a fluence-dependent shift towards the surface, with broadening near the surface. Accordingly, existence of the narrowing effect suggests another mechanism of atomic transport. It is also noted that the total Cu amount in the precipitates is less than a half of the nominal amount of the implants. On the contrary, Fig. 2(c) of $MgO \cdot 2.4(Al_2O_3)$ indicates no occurrence of anomalous redistribution along the depth, even at high fluxes, whereas the total Cu amount in nanoparticles agrees with the TRIM code. Consequently, the $MgO \cdot 2.4(Al_2O_3)$ causes radiation-induced diffusion enough to fully precipitate, but the long-range atomic transport does not occur. This precipitation behavior is consistent with the presence of abundant recombination sites for defects in $MgO \cdot 2.4(Al_2O_3)$ [12].

Radiation-induced atomic transport is diagnosed by ion-induced photon spectroscopy. Fig. 3(a) shows fluence dependence of emission spectra of a-SiO_2 during implanted with 60 keV Cu^- at 50 μA/cm^2. The ion-induced photon spectra consist of sharp line spectra and a broad luminescence around 560 nm (IIL). The line spectra imply isolated atomic states released from the solid. The line intensities of Si-I at 288.2 nm and Cu-I at 324.8 nm [15] are plotted as a function of fluence. The luminescence increases with increasing defects and decayed with further increasing fluence, which reflects from production and subsequent non-radiative decay of luminescent centers. The line spectra clearly demonstrated the outward atomic transport of isolated atoms, Si and Cu, via the surface into the vacuum. While the Si line keeps a constant level, the Cu line manifests a characteristic variation with fluence. The atomic release

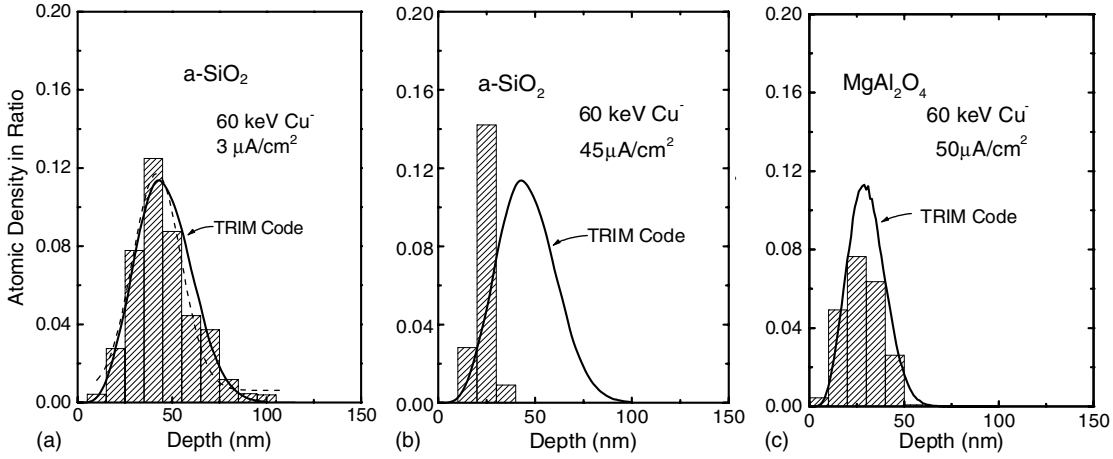

Fig. 2. Depth profiles of Cu atoms in a-SiO_2 at 3 μA/cm^2 (a), 45 μA/cm^2 (b) and in $MgO \cdot 2.4(Al_2O_3)$ at 50 μA/cm^2 (c). The Cu amount was statistically evaluated from TEM photographs assuming Cu nanocrystals.

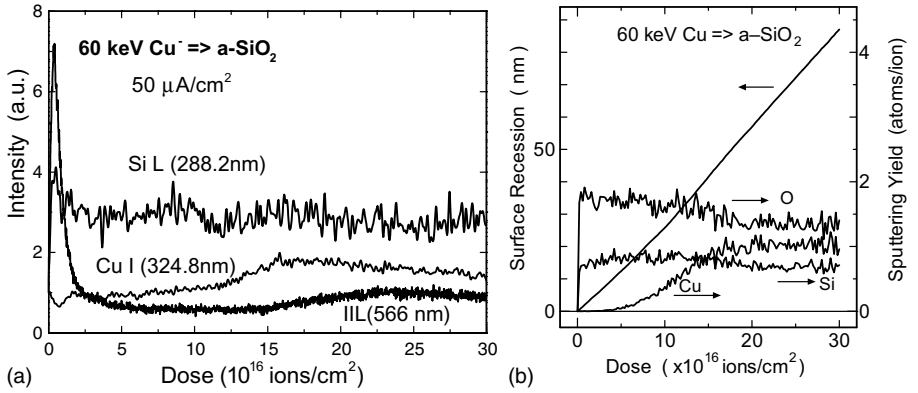

Fig. 3. Fluence dependence of emission spectra of a-SiO_2 during implanted with 60 keV Cu^- at 50 μA/cm^2 (a) in comparison with that calculated by the TRIDYN code [14].

indicates pronounced loss of Cu atoms particularly above 1.5×10^{17} ions/cm^2. Fig. 3(b) shows the fluence dependence of Si, O and Cu atoms sputtered from the surface, after the TRIDYN calculation. The fluence-dependent atomic release of Si and Cu qualitatively agrees between the experimental results and the theoretical calculation. In particular, the onset fluence of Cu release above 1.5×10^{17} ions/cm^2 is well explained by the TRIDYN code. Accordingly, the physical sputtering process of the heavily-implanted substrate may be the major mechanism of the ion-induced atomic release. However, there are a few points which cannot be explained by the ordinary sputtering regime: Firstly, the ion-induced photon spectra increase non-linearly with flux, and result from flux dependent variations of Cu profile, i.e. Cu retention (Figs. 2(a) and (b)). Secondly, the Cu release begins earlier than the onset around 1.5×10^{17} ions/cm^2. Finally, the Cu-depleted zone just beneath the surface (Fig. 2(b) always exists up to the higher fluence, while the TRIDYN code predicts a finite distribution in the vicinity of the surface. These results indicate participation of another mechanism in the surface atomic release enhanced by energy-deposition rate. Since the additional mechanism is not associated with physical collisions, the process can be named as ion-energy enhanced sublimation of implants. This mechanism is important to understand the whole atomic transport in the high-flux implantation. The Cu-depleted zone beneath the surface, which results in narrowing of the Cu depth profile, and the larger loss of implants can be explained by this mechanism. It should be emphasized for a-SiO_2 that the outward atomic transport uniquely affects the depth distribution of nanoparticles.

Fig. 4(a) shows fluence dependence of emission spectra of $MgO\cdot2.4(Al_2O_3)$ implanted with 60 keV Cu^- at 100 μA/cm^2 in comparison with that of the TRIDYN calculation. The line intensities of Al-I at 396.2, Mg-I at 518.4 nm and the ratio of (Al-I)/(Mg-I) are plotted as a function of fluence. The TRIDYN considerably explains fluence dependence of atomic release of Al and Mg. Since the original composition is rich in Al atoms, the atomic release of Al is quantitatively larger than that of Mg. Up to 3.0×10^{17} ions/cm^2, no saturation of either Al or Mg takes place and the ratio of (Al-I)/(Mg-I) gradually increases with the total fluence, that is, the Mg release decays faster than the Al release. The result indicates that Mg-depleted zone first forms and keeps changing the stoichiometry of the surface layer.

4. Summary

Negative Cu ions of 60 keV were implanted to a-SiO_2 and $MgO\cdot2.4(Al_2O_3)$ up to high fluxes and Cu nanoparticles, with a variety of morphology, were spontaneously fabricated. Comparison

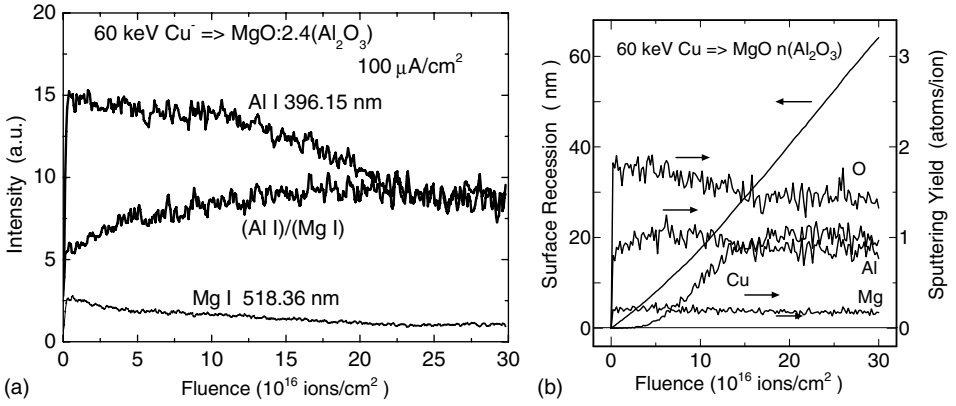

Fig. 4. Fluence dependence of line emission spectra of $MgO \cdot 2.4(Al_2O_3)$ during implanted with 60 keV Cu^- at 100 μA/cm^2 (a) in comparison with that calculated by the TRIDYN code [14].

between X-TEM and ion-induced photon spectroscopy revealed significant atomic transports inside and outside of the substrate at high fluxes. The atomic transports were dependent on substrate species and effected on the resultant nanoparticle morphology. In a-SiO_2, not only radiation-induced diffusion but also the depth-oriented atomic transport caused shallowing and narrowing of the Cu implants. The narrowing effect was enhanced by formation of the near-surface depleted zone, which resulted from the outward atomic transport due to enhanced surface sputtering and/or sublimation. In $MgO \cdot 2.4(Al_2O_3)$, the intra-solid atomic transport of implants was not so significant but the original distribution of implants was maintained, which was consistent with the absence of long-range diffusion of implants.

Acknowledgements

A part of this study was financially supported by the Budget for Nuclear Research of the MEXT, based on the screening and counseling by the Atomic Energy Commission. The authors are grateful to Dr. H. Amekura of NIMS for useful discussion and to Ms. J. Lu for preparation of the X-TEM specimens.

References

[1] J.-Y. Bigot, J.-C. Merle, O. Cregut, A. Daunois, Phys. Rev. Lett. 75 (1995) 4702.
[2] R.F. Haglund Jr., Mater. Sci. Eng. A 253 (1998) 275.
[3] J. Ishikawa, H. Tsuji, Y. Toyota, Y. Gotoh, K. Matsuda, M. Tanjyo, S. Sakaki, Nucl. Instr. and Meth. B 96 (1995) 7.
[4] N. Kishimoto, Y. Takeda, V.T. Gritsyna, E. Iwamoto, T. Saito, in: Proceedings of the 12th International Conference on Ion Implantation Technology, IEEE, Ion Implantation Technology, Vol. 12, 1999, p. 342.
[5] N. Kishimoto, N. Umeda, Y. Takeda, C.G. Lee, V.T. Gritsyna, Nucl. Instr. and Meth. B 148 (1999) 1017.
[6] N. Kishimoto, Y. Takeda, N. Umeda, V.T. Gritsyna, C.G. Lee, T. Saito, Nucl. Instr. and Meth. B 166–167 (2000) 840.
[7] E. Valentin, H. Bernas, C. Ricolleau, F. Creuzet, Phys. Rev. Lett. 86 (2001) 99.
[8] Y. Takeda, V.T. Gritsyna, N. Umeda, C.G. Lee, N. Kishimoto, Nucl. Instr. and Meth. B 148 (1999) 1029.
[9] H. Hosono, H. Fukushima, Y. Abe, R.A. Weeks, R.A. Zuhr, J. Non-Cryst. Solids 143 (1992) 157.
[10] R.H. Magruder III, R.F. Haglund Jr., L. Yang, J.E. Wittig, R.A. Zuhr, J. Appl. Phys. 76 (1994) 708.
[11] M.L. Brongersma, E. Snoeks, A. Polman, Appl. Phys. Lett. 71 (1997) 1628.
[12] C. Kinoshita, J. Nucl. Mater. 191–194 (1992) 67.
[13] J.F. Ziegler, J.P. Biersack, U. Littmark, The Stopping and Range of Ions in Solids, Pergamon Press, New York, 1985, Chapter 8.
[14] W. Moeller, W. Eckstein, Nucl. Instr. and Meth. B 2 (1984) 814.
[15] W.F. Van der Weg, D.J. Bierman, Physica 44 (1969) 206.